SCIENTIFIC REP⊙RTS

OPEN

Indium phosphide metasurface with enhanced nonlinear absorption

Brian Slovick, Lucas Zipp & Srini Krishnamurthy

We solve the nonlinear Maxwell equations in an InP-based dielectric metamaterial, considering both two-photon absorption and photo-induced free-carrier absorption. We obtain the intensity-dependent reflection, absorption, and effective permittivity and permeability of the metamaterial. Our results show that nonlinear absorption dampens both the electric and magnetic Mie resonance, although the magnetic resonance is more affected because it occurs at longer wavelengths where the free-carrier absorption cross section is larger. Owing to field concentration in the metamaterial at resonance, the threshold intensity for nonlinear absorption is reduced by a factor of about 30 compared to a homogeneous layer of the same thickness. Our results have implications on the use of dielectric metamaterials for nonlinear applications such as higher harmonic generation, optical limiting, and ultrafast modulation.

Materials with strong nonlinear response are desired for applications such as optical limiting[1–3], ultrafast modulation[4–6], frequency conversion[7,8], and optical isolation[9,10]. Traditional bulk materials have a weak interaction between electrons and sub-bandgap photons, as measured by nonlinear absorption coefficients[11–14], and thus require high intensities or long interaction lengths to achieve an efficient nonlinear response.

One way to enhance the nonlinear response is to incorporate metamaterial elements or plasmonic structures to concentrate the electric fields within a nonlinear material[15,16]. Metamaterials containing plasmonic nanostructures have been integrated with nonlinear materials to enhance second-harmonic generation[17–23] and achieve analog electromagnetically induced transparency[24,25]. The drawback of plasmonic approaches is that the fields are highly localized at the metal dielectric interface, leading to small interaction volumes[26]. Also, the finite conductivity of metals at optical frequencies leads to undesirable losses. An alternative approach is to induce nonlinearity in dielectric metamaterials using Mie resonances[27]. Field enhancement in dielectric metamaterials has been demonstrated[27] and applied to achieve third-harmonic generation[26,28–32], optical limiting[33], and ultrafast optical modulation[34–36].

To obtain efficient harmonic generation or optical modulation, the materials involved must be transparent at high intensities. However, at high intensities nonlinear absorption processes such as two photon absorption (TPA) and free-carrier absorption (FCA) become significant[1,14]. Therefore, in order to optimize nonlinear effects in dielectric metamaterials it is important to understand the role of nonlinear absorption. To date, the research has focused primarily on the experimental aspects[26,28–32], with relatively few examples of theoretical studies. A few examples employ the recently-developed generalized source method for nonlinear materials[37–39], which calculates the diffraction by periodic structures containing linear and nonlinear media. Although these models provide important insights, they decouple the linear and nonlinear responses, and thus do not represent self-consistent solutions of the nonlinear Maxwell equations. Also, existing models[33] do not account for the nontrivial frequency dependence of the nonlinear parameters, such as the TPA coefficient and the FCA cross section[14].

In this work, we develop a full-wave model to solve the nonlinear Maxwell equations in a dielectric metamaterial accounting for both TPA and photo-induced FCA. We apply the model to study the optical properties and effective parameters of a representative indium phosphide (InP)-based dielectric metamaterial operating in the near infrared spectral band. We find that nonlinear absorption leads to damping of the electric and magnetic Mie resonances at high intensities. For continuous wave illumination, the onset of nonlinear absorption occurs at intensities of $1\,MW/cm^2$, while the Mie resonances are almost completely diminished for intensities approaching $5\,MW/cm^2$. We also find several unexpected results. First, due to the wavelength dependence of FCA, the nonlinear

SRI International, Applied Optics Laboratory, Menlo Park, CA, 94025, United States. Correspondence and requests for materials should be addressed to B.S. (email: brian.slovick@sri.com)
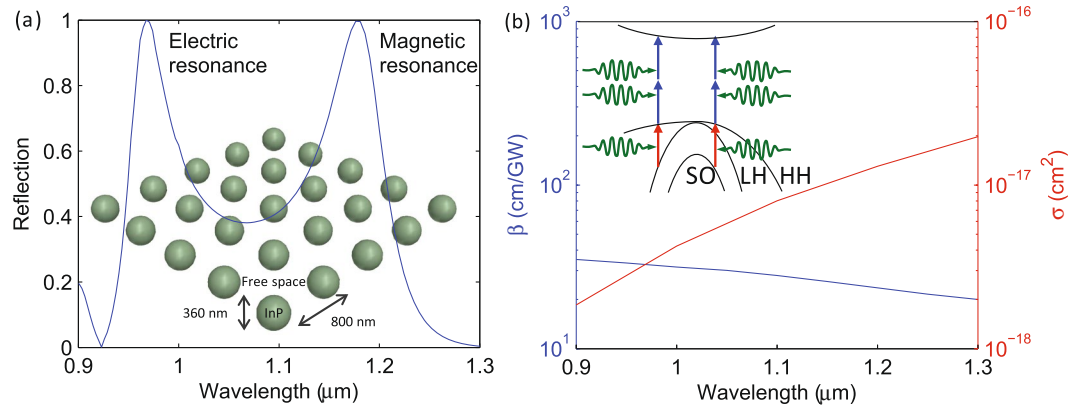
1

Figure 1. (**a**) Dielectric metamaterial consisting of InP spheres in free space and the calculated reflection spectrum for low intensities, showing two peaks corresponding to the electric and magnetic Mie resonances. (**b**) Electronic band structure of InP, showing heavy hole (HH), light hole (LH), and spin orbit (SO) bands, and the wavelength dependence of the two-photon absorption coefficient (β) and free-carrier absorption cross section (σ) obtained from full band structure calculations[14]. The blue and red arrows, respectively, illustrate two-photon and free carrier absorption.

absorption at the magnetic resonance is larger than at the electric resonance. Second, assuming FCA is independent of wavelength, the absorption at the two resonances is found to be nearly equal, despite the electric field being heavily localized at the electric resonance and more uniformly distributed at the magnetic resonance. Third, owing to the enhancement of the electric field at resonance, we find that the intensity threshold of nonlinear absorption in the metamaterial is nearly 30 times lower compared to a homogeneous material of the same thickness.

Methods

Metamaterial design. To clearly illustrate the effects of nonlinearity on Mie resonances, we consider a large index-contrast metamaterial consisting of 360 nm InP spheres with large refractive index (3.3 at 1 μm) in air medium, arranged in a square lattice with a periodicity of 800 nm, as shown in inset of Fig. 1(a). InP is chosen for its transparency in the near-infrared band of interest (0.9–1.3 μm). Note the conclusions drawn in this article remain valid when the air medium is replaced by a polymer and the metamaterial layer is placed on a low index substrate such as silica. The size and periodicity of the InP spheres are optimized to position the electric and magnetic Mie resonances, identified as narrowband peaks in the reflection spectrum, in the band of interest as shown in Fig. 1(a).

The origin of nonlinear absorption in InP can be understood from the band structure, shown in Fig. 1(b). The valence bands (VBs) consist of heavy-hole (HH), light-hole (LH), and spin-orbit (SO) bands. The conduction band (CB) is separated from the HH band by the band gap. In the absence of light, states in the VB are filled with electrons and the CB states are empty. Electrons in the VB can enter the CB by absorbing photons with energy larger than the band gap. Since the band gap of InP (1.45 eV) is larger than the photon energies in the band of interest (0.95–1.4 eV), at low intensities photons transmit through InP without being absorbed. However, when the incident intensity is large, the probability for valence electrons to absorb two photons (shown as two stacked vertical blue arrows) is high, resulting in reduced transmission. In addition, this TPA is followed by FCA in which the holes left behind in the HH band can be filled by one-photon absorption of electrons in the LH and SO bands, shown by the red arrows in Fig. 1(b). Because the strength of TPA and FCA depend on intensity, they are referred to as nonlinear absorption processes. There can also be Drude-like FCA by conduction electrons (not shown). However, this process requires both a photon and phonon to conserve energy and momentum, whereas the FCA considered in our studies is a one-photon process with a cross section two orders of magnitude larger[14]. We also note that for the highest intensities considered in this work, the carrier density in InP is less than 10^{18} cm^{-3}, corresponding to a plasma wavelength greater than 50 μm, which is considerably higher than near-infrared wavelengths. Therefore, we neglect FCA due to conduction electrons and the electron-hole plasma. Figure 1(b) also shows the previously calculated values of the TPA coefficient β and FCA cross section σ of InP[14]. The value of β is relatively constant with wavelength, which is typical for wide-bandgap materials, while σ increases by an order of magnitude over the band. The FCA increases with increasing wavelength because the corresponding photon energy decreases, and the energy-momentum conservation condition for FCA (red lines in Fig. 1(b)) is satisfied only near the center of the Brillouin zone, where a larger number of holes are present.

Nonlinear full-wave modeling. We will now incorporate these nonlinear coefficients into Maxwell's equations. The nonlinear Maxwell equation for the electric field $\mathbf{E}(\mathbf{r}, t)$ is[40,41]

$$\left(\nabla^2 - \frac{n^2}{c^2}\frac{\partial^2}{\partial t^2} - \frac{n\sigma N}{c}\frac{\partial}{\partial t}\right)\mathbf{E}(\mathbf{r},\, t) = \frac{1}{\varepsilon_0 c^2}\frac{\partial^2 \mathbf{P}_{NL}(\mathbf{r},\, t)}{\partial t^2}, \tag{1}$$

where n is the refractive index, c is the speed of light, N and σ are the free-carrier concentration and absorption cross section, ε_0 is the free-space permittivity, and $\mathbf{P}_{NL}(\mathbf{r},\, t)$ is the nonlinear polarization. Taking the Fourier

transform of Eq. ([1]), assuming an $\exp(-i\omega t)$ time dependence, and using the relation for the third-order nonlinear polarization

$$\mathbf{P}_{NL}(\mathbf{r},\,\omega) = \frac{3}{4}\varepsilon_0\chi^{(3)}(\omega)|\mathbf{E}(\mathbf{r},\,\omega)|^2\mathbf{E}(\mathbf{r},\,\omega),$$

(2)

where $\chi^{(3)}$ is the nonlinear susceptibility, we obtain

$$\left(\nabla^2 + n^2\frac{\omega^2}{c^2} + \frac{3}{4}\frac{\omega^2}{c^2}\chi^{(3)}|\mathbf{E}(\mathbf{r},\,\omega)|^2 + i\omega\frac{n\sigma N}{c}\right)\mathbf{E}(\mathbf{r},\,\omega) = 0.$$

(3)

Relating the imaginary part of $\chi^{(3)}$ to the two-photon absorption coefficient β as[40,41]

$$\text{Im}(\chi^{(3)}) = \frac{2n^2c^2\varepsilon_0}{3\omega}\beta,$$

and neglecting the relatively small real part of $\chi^{(3)}$[14], Eq. ([3]) can be rewritten as

$$\left(\nabla^2 + n^2\frac{\omega^2}{c^2} + i\frac{1}{2}\beta\omega n^2\varepsilon_0|\mathbf{E}(\mathbf{r},\,\omega)|^2 + i\omega\frac{n\sigma N}{c}\right)\mathbf{E}(\mathbf{r},\,\omega) = 0.$$

(4)

The free carrier concentration is given by the continuity equation for free electrons[14,40,41]

$$\frac{\partial N}{\partial t} = \frac{\beta I^2}{2\hbar\omega} - \frac{N}{\tau},$$

(5)

where $I = \frac{1}{2}nc\varepsilon_0|\mathbf{E}(\mathbf{r},\,\omega)|^2$ is the intensity, $\hbar\omega$ is the photon energy and τ is the photo-carrier relaxation time. The first term in Eq. ([5]) describes free-carrier generation via TPA, and the second term describes free carrier recombination. For continuous-wave illumination, the free-carrier concentration will reach steady state conditions ($\partial N/\partial t = 0$) and thus

$$N(I) = \frac{\beta\tau}{2\hbar\omega}I^2.$$

(6)

In pure InP, defect-mediated Shockley–Read–Hall lifetimes exceed 10 ms, and radiative recombination lifetimes are effectively long due to photon recycling (i.e., emission and re-absorption)[14]. The limiting lifetime is associated with Auger recombination, which dominates at higher carrier densities, or equivalently, higher intensities. The lifetime associated with nonradiative Auger recombination is given by $1/(CN^2)$, where C is the Auger recombination coefficient ($=10^{-30}$ cm^6/s for InP)[14]. Using the expression in Eq. ([6]) for the carrier concentration under steady state conditions, for the highest intensity consider in this work (5 MW/cm^2), we calculate an equilibrium carrier density of 10^{18} cm^{-3}, which corresponds to a lifetime of 0.6 μs. At lower intensities, the lifetime is longer owing to lower carrier densities. We assume a constant lifetime of 1 μs, near the lower end of the range.

Substituting Eq. ([6]) into Eq. ([4]), we obtain the following form of the nonlinear Maxwell equation:

$$(\nabla^2 + n^2\frac{\omega^2}{c^2} + i\frac{1}{2}\beta\omega n^2\varepsilon_0|\mathbf{E}(\mathbf{r},\,\omega)|^2 + i\frac{\sigma\beta\tau n^3 c\varepsilon_0^2}{8\hbar}|\mathbf{E}(\mathbf{r},\,\omega)|^4)\mathbf{E}(\mathbf{r},\,\omega) = 0.$$

(7)

We solve Eq. ([7]) using the full-wave finite-element frequency domain solver in COMSOL Multiphysics. This was accomplished by assigning the two nonlinear terms in Eq. ([7]) to the imaginary part of n^2. Before solving Eq. ([7]) in the metamaterial in Fig. [1], we apply it to a homogeneous nonlinear medium and compare the results with the solution to the well-known rate equation[40,41]

$$\frac{dI}{dx} = -\beta I^2 - \frac{\sigma\beta\tau}{2\hbar\omega}I^3.$$

(8)

The transmitted intensity, as a function of thickness for InP at a wavelength of 1 μm for various intensities, calculated by solving Eqs ([7]) and ([8]), respectively, are shown by dots and solid lines in Fig. [2]. The two calculations are in excellent agreement, thus validating our full-wave nonlinear model. In this validation the index of InP is set equal to 1 to avoid interference effects, which are not included in Eq. ([8]).

Data availability statement. The datasets generated during and/or analysed during the current study are available from the corresponding author on reasonable request.

Results

Optical properties. We now apply our validated nonlinear full-wave model [(Eq. ([7])] to understand the role of nonlinear absorption in the dielectric metamaterial shown in Fig. [1]. First, we studied the reflection and absorption for different incident intensities, shown in Fig. [3]. For all intensities, the reflection spectrum contains narrowband peaks near 1.2 and 0.95 μm, corresponding to the magnetic and electric dipole Mie resonances, respectively. For a low intensity of 1 W/cm^2, the nonlinear processes are negligible, resulting in low absorption and nearly 100% reflection at the two resonances. As the intensity increases, the absorption at the resonances increases and the reflection decreases.
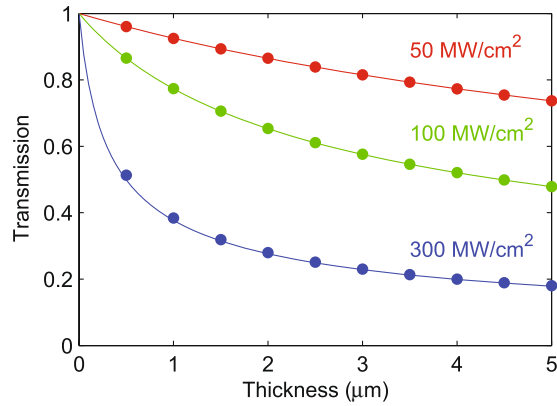
Figure 2. Transmission of bulk InP at 1 μm as a function of thickness for different incident intensities, calculated using nonlinear full-wave COMSOL (dots) and by numerically integrating Eq. (8) (solid lines).
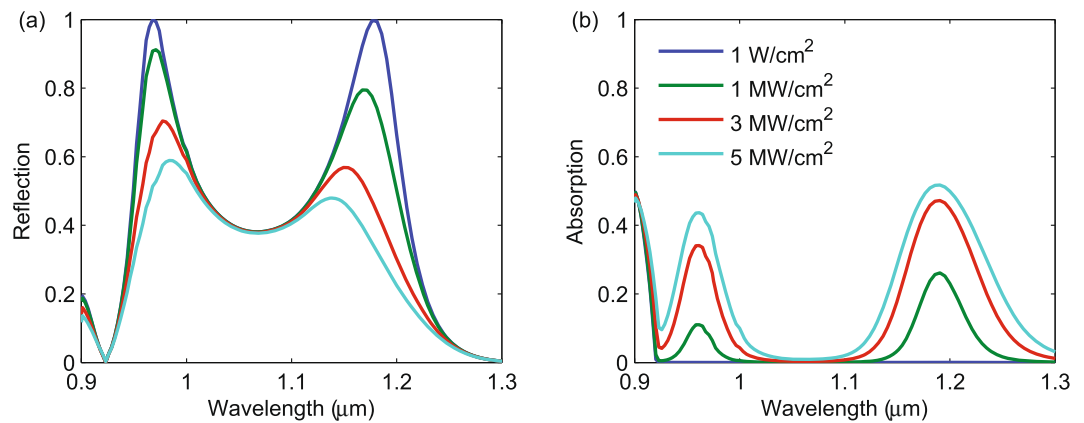

Figure 3. Wavelength dependence of the reflection (**a**) and absorption (**b**) for a 0.8 μm square array of 360-nm diameter InP spheres for different incident intensities.

We note that for a given intensity, the absorption is larger at the magnetic resonance (1.2 μm) than at the electric resonance (0.95 μm). This is a surprising result considering the electric field distributions at the resonances, shown in the inset of Fig. 4, normalized to the incident electric field for an intensity of 1 MW/cm². At the magnetic dipole resonance, the electric field is ring shaped and relatively uniform, while the electric field at the electric dipole resonance is highly concentrated at the center of the sphere. Note the field concentration outside the sphere arises from the boundary condition on the normal component electric field, which is discontinuous by the ratio of the dielectric constants of the sphere and free space[42]. Thus, based on the field distributions, one might expect the absorption at the electric resonance to be larger due to the larger field concentration. However, we find more absorption at the magnetic resonance. We attribute this to the FCA cross section being about 5 times larger at the magnetic resonance than at the electric resonance [Fig. 1(b)]. To validate this claim, we recalculated the spectral absorption for 1 MW/cm² intensity, assuming a constant FCA cross section. The results, shown in Fig. 4, indicate that the absorption is approximately equal at the two resonances, confirming that the wavelength-dependent FCA cross section is responsible for the larger absorption at the magnetic resonance.

The fact that the absorption is equal at the two resonances for constant FCA is also counterintuitive, since more absorption is expected at the electric resonance because of the larger field concentration. In fact, we find that $|E|^2$ integrated over the sphere is 1.5 times larger at the electric resonance than at the magnetic resonance. Despite this, the absorption is equal at the two resonances for constant free carrier absorption cross section. In materials with complex permittivity ($\varepsilon = \varepsilon' + i\varepsilon''$), absorption is given by the volume integral of $\varepsilon''|E|^2$. Noting that $\varepsilon'' = 2nk$, where n and k are the components of the complex refractive index $n + ik$, where k is given by $\sigma N\lambda/(4\pi)$ and from Eq. (6), $N = \beta\tau I^2\lambda/(2hc)$, we find that ε'' is proportional to wavelength squared. Thus, ε'' is (1.2 μm/0.97 μm)² = 1.5 times larger at the magnetic resonance, leading to equal absorption at the two resonances when σ is independent of wavelength.

Since the electric field is enhanced at both resonances, we expect more absorption per unit length in the metamaterial than in a homogeneous material. To illustrate this, we calculated the reflection and absorption of a 360 nm-thick slab of InP, equal in thickness to the InP sphere metamaterial in Fig. 1. We see from Fig. 5 that 100 MW/cm² of intensity is needed to obtain 40% absorption near 1.2 μm in the homogeneous layer, whereas the
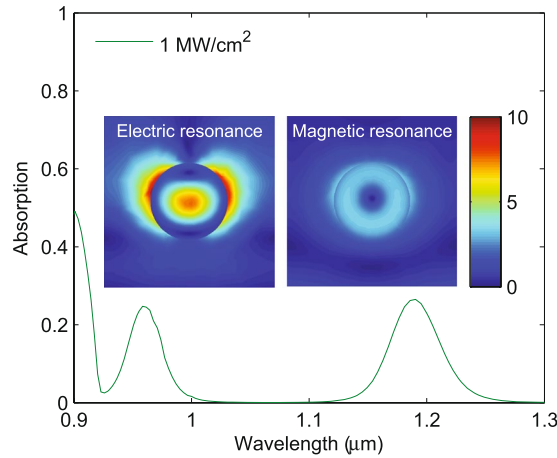
Figure 4. Electric field distributions, normalized to the incident field, at the electric and magnetic resonance for an incident intensity of 1 MW/cm², and the absorption of the metamaterial for an intensity of 1 MW/cm², assuming a constant free carrier absorption cross section.
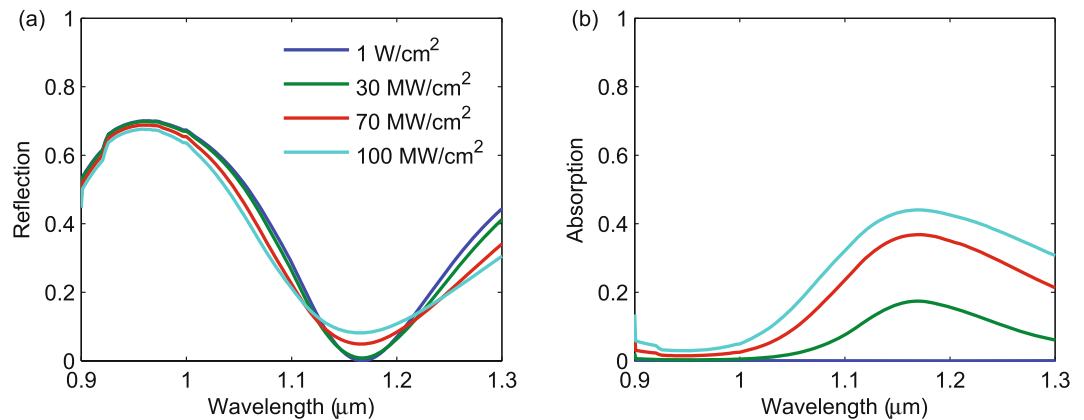

Figure 5. Wavelength dependence of the reflection (**a**) and absorption (**b**) for a 360 nm thick film of InP for different incident intensities.

metamaterial obtains a similar level of absorption for 3 MW/cm². Thus, the homogeneous layer requires much higher intensities to achieve absorption values comparable to the metamaterial. This factor of 30 higher intensity is consistent with the five-fold field enhancement at the magnetic resonance shown in Fig. 4.

Metamaterial parameters. It is also important to understand the impact of nonlinear absorption on the effective permittivity (ε) and permeability (μ) of the metamaterial, as ε and μ are often used to obtain unique properties such as negative refraction[43] and perfect reflection[44]. The calculated real parts of ε and μ, shown in Fig. 6, were obtained using S-parameter inversion, assuming a layer thickness of 1.24 μm. At low intensities, shown as the blue line in Fig. 6(a), we see a strong resonance in μ near 1.2 μm, which arises from the magnetic resonance. The weaker resonance near 0.95 μm is the anti-resonance associated with the strong electric resonance at that wavelength, clearly seen in Fig. 6(b) for the permittivity. We also find a strong anti-resonance in ε at 1.1 μm, which arises from the magnetic resonance at 1.2 μm. These anti-resonances are an artifact of S-parameter retrieval that arises from approximating a Bloch wave by a plane wave[45]. In the resonance regions, either ε or μ is negative, resulting in single-negative regions and high reflectivity, as shown in Fig. 3(a). As the intensity increases to 1 MW/cm² and 3 MW/cm², we find that the magnetic resonance, near 1.2 μm in Fig. 6(a), begins to dampen while the electric resonance, near 1 μm in Fig. 6(b), is largely unchanged. Only when the intensity exceeds 3 MW/cm² does the electric resonance begin to dampen. For 5 MW/cm², both resonances are completely dampened. As the resonance in the real part of ε and μ broadens, the corresponding imaginary parts of ε and μ (not shown) also broaden, as per the Kramer-Kronig relationship, which results in broader-band absorption with increasing intensity, as shown in Fig. 3(b).

Discussion

In summary, we developed a self-consistent full-wave model to study the effects of two-photon absorption and photo-induced free-carrier absorption on the effective parameters and optical properties of a dielectric metamaterial operating in the near infrared spectral band. As expected, we find that nonlinear absorption leads to
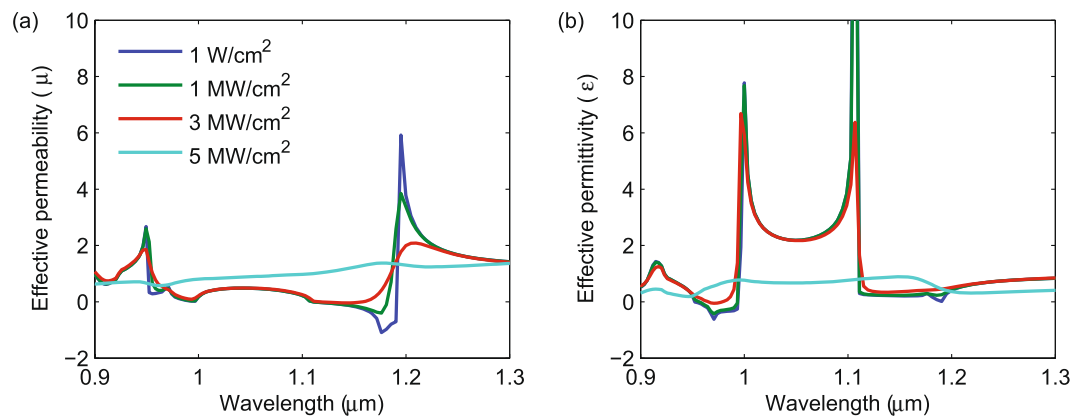
Figure 6. Wavelength dependence of the effective permeability (**a**) and permittivity (**b**) of the InP metamaterial for different incident intensities.

damping of the electric and magnetic Mie resonances at high intensities, with an onset around $1\,MW/cm^2$ for continuous wave illumination. The resonances are almost completely dampened for intensities around $5\,MW/cm^2$. Surprisingly, we find that the nonlinear absorption at the magnetic resonance is larger than at the electric resonance, despite the electric field being more concentrated at the electric resonance. We find this is because the free-carrier absorption cross section is considerably larger at the longer wavelengths near the magnetic resonance. We also find that the metamaterial provides absorption comparable to a homogeneous layer of the same thickness at approximately 30 times less intensity. The lower threshold intensity and smaller footprint for nonlinear absorption have implications on the use of dielectric metamaterials for nonlinear applications such as optical limiting, higher harmonic generation, and ultrafast modulation.

References

1. Stryland, E. W. V. *et al.* Two-photon absorption, nonlinear refraction and optical limiting in semiconductors. *Opt. Eng.* **24**, 613–623 (1985).
2. Boggess, T., Smirl, A., Moss, S., Boyd, I. & Stryland, E. V. Optical limiting in GaAs. *IEEE J. Quant. Electron.* **21**, 488–494 (1985).
3. Stryland, E. W. V., Wu, Y. Y., Hagan, D. J., Soileau, M. J. & Mansour, K. Optical limiting with semiconductors. *JOSA B* **5**, 1980–1988 (1988).
4. Scalora, M., Dowling, J. P., Bowden, C. M. & Bloemer, M. J. Optical limiting and switching of ultrashort pulses in nonlinear photonic band gap materials. *Phys. Rev. Lett.* **73**, 1368–1371 (1994).
5. Tran, P. Optical limiting and switching of short pulses by use of a nonlinear photonic bandgap structure with a defect. *JOSA B* **14**, 2589–2595 (1997).
6. Hache, A. & Bourgeois, M. Ultrafast all-optical switching in a silicon-based photonic crystal. *Appl. Phys. Lett.* **77**, 4089–4091 (2000).
7. Rashkeev, S. N. & Lambrecht, W. R. Second-harmonic generation of I-III-VI$_2$ chalcopyrite semiconductors: Effects of chemical substitutions. *Phys. Rev. B* **63**, 165212 (2001).
8. Lekse, J. M. *et al.* Second-harmonic generation and crystal structure of the diamond-like semiconductors Li$_2$CdGeS$_4$ and Li$_2$CdSnS$_4$. *Inorg. Chem.* **48**, 7516–7518 (2009).
9. Gallo, K. & Assanto, G. All-optical diode based on second-harmonic generation in an asymmetric waveguide. *JOSA B* **16**, 267–269 (1999).
10. Yu, Z. & Fan, S. Complete optical isolation created by indirect interband photonic transitions. *Nat. Photon.* **3**, 91–94 (2009).
11. Chang, D. E., Vuletic, V. & Lukin, M. D. Quantum nonlinear optics-photon by photon. *Nat. Photon.* **8**, 685–694 (2014).
12. Bechtel, J. H. & Smith, W. L. Two-photon absorption in semiconductors with picosecond laser pulses. *Phys. Rev. B* **13**, 3515 (1976).
13. Boggess, T. *et al.* Simultaneous measurement of the two-photon coefficient and free-carrier cross section above the bandgap of crystalline silicon. *IEEE J. Quant. Electron.* **22**, 360–368 (1986).
14. Krishnamurthy, S., Yu, Z. G., Gonzalez, L. P. & Guha, S. Temperature-and wavelength-dependent two-photon and free-carrier absorption in GaAs, InP, GaInAs, and InAsP. *J. Appl. Phys.* **109**, 033102 (2011).
15. Kauranen, M. & Zayats, A. V. Nonlinear plasmonics. *Nat. Photon.* **6**, 737–748 (2012).
16. Schuller, J. A. *et al.* Plasmonics for extreme light concentration and manipulation. *Nat. Mater.* **9**, 193 (2010).
17. Czaplicki, R. *et al.* Enhancement of second-harmonic generation from metal nanoparticles by passive elements. *Phys. Rev. Lett.* **110**, 093902 (2013).
18. Aouani, H. *et al.* Multiresonant broadband optical antennas as efficient tunable nanosources of second harmonic light. *Nano Lett.* **12**, 4997–5002 (2012).
19. Thyagarajan, K., Rivier, S., Lovera, A. & Martin, O. J. Enhanced second-harmonic generation from double resonant plasmonic antennae. *Opt. Exp.* **20**, 12860–12865 (2012).
20. Thyagarajan, K., Butet, J. & Martin, O. J. Augmenting second harmonic generation using fano resonances in plasmonic systems. *Nano Lett.* **13**, 1847–1851 (2013).
21. Zhang, Y., Grady, N. K., Ayala-Orozco, C. & Halas, N. J. Three-dimensional nanostructures as highly efficient generators of second harmonic light. *Nano Lett.* **11**, 5519–5523 (2011).
22. Harutyunyan, H., Volpe, G., Quidant, R. & Novotny, L. Enhancing the nonlinear optical response using multifrequency gold-nanowire antennas. *Phys. Rev. Lett.* **108**, 217403 (2012).
23. Navarro-Cia, M. & Maier, S. A. Broad-band near-infrared plasmonic nanoantennas for higher harmonic generation. *ACS Nano* **6**, 3537–3544 (2012).
24. Gu, J. *et al.* Active control of electromagnetically induced transparency analogue in terahertz metamaterials. *Nat. Comm.* **3**, 1151 (2012).
25. Kurter, C. *et al.* Classical analogue of electromagnetically induced transparency with a metal-superconductor hybrid metamaterial. *Phys. Rev. Lett.* **107**, 043901 (2011).

26. Yang, Y. *et al*. Nonlinear fano-resonant dielectric metasurfaces. *Nano Lett.* **15**, 7388–7393 (2015).
27. Kapitanova, P. *et al*. Giant field enhancement in high-index dielectric subwavelength particles. *Sci. Rep.* **7**, 731 (2017).
28. Shcherbakov, M. R. *et al*. Enhanced third-harmonic generation in silicon nanoparticles driven by magnetic response. *Nano Lett.* **14**, 6488–6492 (2014).
29. Shcherbakov, M. R. *et al*. Nonlinear interference and tailorable third-harmonic generation from dielectric oligomers. *ACS Photon.* **2**, 578–582 (2015).
30. Smirnova, D. A., Khanikaev, A. B., Smirnov, L. A. & Kivshar, Y. S. Multipolar third-harmonic generation driven by optically induced magnetic resonances. *ACS Photon.* **3**, 1468–1476 (2016).
31. Grinblat, G., Li, Y., Nielsen, M. P., Oulton, R. F. & Maier, S. A. Enhanced third harmonic generation in single germanium nanodisks excited at the anapole mode. *Nano Lett.* **16**, 4635–4640 (2016).
32. Shorokhov, A. S. *et al*. Multifold enhancement of third-harmonic generation in dielectric nanoparticles driven by magnetic fano resonances. *Nano Lett.* **16**, 4857–4861 (2016).
33. Jafar-Zanjani, S., Cheng, J., Liberman, V., Chou, J. B. & Mosallaei, H. Large enhancement of third-order nonlinear effects with a resonant all-dielectric metasurface. *AIP Adv.* **6**, 115213 (2016).
34. Shcherbakov, M. R. *et al*. Ultrafast all-optical switching with magnetic resonances in nonlinear dielectric nanostructures. *Nano Lett.* **15**, 6985–6990 (2015).
35. Makarov, S. *et al*. Tuning of magnetic optical response in a dielectric nanoparticle by ultrafast photoexcitation of dense electron–hole plasma. *Nano Lett.* **15**, 6187–6192 (2015).
36. Baranov, D. G. *et al*. Nonlinear transient dynamics of photoexcited resonant silicon nanostructures. *ACS Photon.* **3**, 1546–1551 (2016).
37. Weismann, M., Gallagher, D. F. & Panoiu, N. C. Nonlinear generalized source method for modeling second-harmonic generation in diffraction gratings. *JOSA B* **32**, 523–533 (2015).
38. Weismann, M. & Panoiu, N. C. Theoretical and computational analysis of second-and third-harmonic generation in periodically patterned graphene and transition-metal dichalcogenide monolayers. *Phys. Rev. B* **94**, 035435 (2016).
39. Kruk, S. *et al*. Enhanced magnetic second-harmonic generation from resonant metasurfaces. *ACS Photon.* **2**, 1007–1012 (2015).
40. Shen, Y. R. *The principles of nonlinear optics* (Wiley-Interscience, 1984).
41. Stegeman, G. I. & Stegeman, R. A. *Nonlinear Optics: Phenomena, Materials and Devices (Vol. 78)* (John Wiley & Sons, 2012).
42. Slovick, B. A. *et al*. Metasurface polarization splitter. *Phil. Trans. R. Soc. A* **375**, 0072 (2017).
43. Smith, D. R., Padilla, W. J., Vier, D. C., Nemat-Nasser, S. C. & Schultz, S. Composite medium with simultaneously negative permeability and permittivity. *Phys. Rev. Lett.* **84**, 4184–4187 (2000).
44. Slovick, B., Yu, Z. G., Berding, M. & Krishnamurthy, S. Perfect dielectric-metamaterial reflector. *Phys. Rev. B.* **88**, 165116 (2013).
45. Koschny, T., Markos, P., Smith, D. R. & Soukoulis, C. M. Resonant and antiresonant frequency dependence of the effective parameters of metamaterials. *Phys. Rev. E* **68**, 065602 (2003).

Acknowledgements

Author Contributions

B.S. and S.K. developed the nonlinear full-wave model. B.S. and L.Z. performed the simulations. B.S. wrote the manuscript. All authors reviewed the manuscript.

Additional Information

Competing Interests: The authors declare that they have no competing interests.

Publisher's note: Springer Nature remains neutral with regard to jurisdictional claims in published maps and institutional affiliations.